ACS SENSORS

pubs.acs.org/acssensors Article

One-Pot Identification of BCR/ABL^{p210} Transcript Isoforms Based on Nanocluster Beacon

Xiaolong Gou,[⊥] Lulu Xu,[⊥] Suqing Yang, Xiaoxue Cheng, Haiping Wu, Decai Zhang, Weicheng Shi, Shijia Ding, Yuhong Zhang,* and Wei Cheng*

Cite This: *ACS Sens.* 2021, 6, 2928−2937 Read Online

ACCESS | Metrics & More | Article Recommendations | Supporting Information

ABSTRACT: The BCR/ABL^{p210} fusion gene is a classic biomarker of chronic myeloid leukemia, which can be divided into e13a2 and e14a2 isoforms according to different breakpoints. These two isoforms showed distinct differences in clinical manifestation, treatment effect, and prognosis risk. Herein, a strategy based on nanocluster beacon (NCB) fluorescence was developed to identify the e13a2 and e14a2 isoforms in one-pot. Because the fluorescence of AgNCs can be activated when they are placed in proximity to the corresponding enhancer sequences, thymine-rich (T-rich) or guanine-rich (G-rich). In this work, we explored an ideal DNA−AgNCs template as an excellent molecular reporter with a high signal-to-noise ratio. After recognition with the corresponding isoforms, the AgNCs can be pulled closer to the T-rich or G-rich sequences to form a three-way junction structure and generate fluorescence with corresponding wavelengths. Therefore, by distinguishing the corresponding wavelengths of AgNCs, we successfully identified two isoforms in one tube with the limitation of 16 pM for e13a2 and 9 pM for e14a2. Moreover, this strategy also realized isoform identification in leukemia cells and newly diagnosed CML patients within 40 min, which provides a powerful tool to distinguish fusion gene subtypes at the same time.

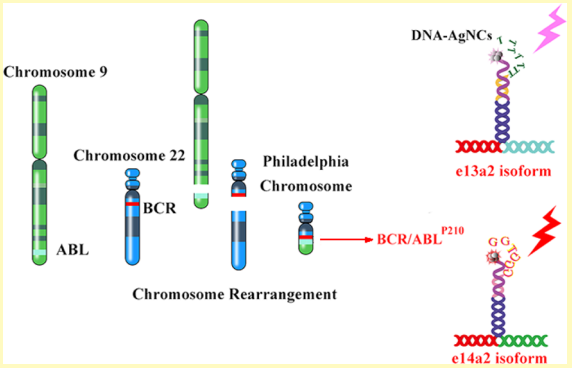

KEYWORDS: *biosensor, AgNCs, fluorescence assay, BCR/ABL^{p210} fusion gene, chronic myeloid leukemia*

The BCR/ABL^{p210} fusion gene is present in more than 95% of chronic myelogenous leukemia (CML) patients,[1,2] which is the result of the translocation between chromosomes 9 and 22.[3−8] Depending on the location of the breakpoint site within the BCR gene, the BCR/ABL^{p210} fusion gene has two important isoforms e13a2 and e14a2.[9] It has been reported that the clinical manifestation and prognosis of e14a2 and e13a2 isoforms are extremely distinct, although their length of transcript sites differs only by 75 bp (25 amino acids).[10] Moreover, they also have different responses to the target drug imatinib, a tyrosine kinase inhibitor, and the e14a2 isoform shows a better therapeutic effect.[11] Compared with the e14a2 isoform patients of CML, patients with the e13a2 isoform have a poorer prognosis and a higher recurrence rate. Therefore, there is an important clinical value to distinguish the e13a2 and e14a2 isoforms of the BCR/ABL^{p210} fusion gene in disease classification and prognosis evaluation.

At present, fluorescence *in situ* hybridization (FISH)[12] and quantitative reverse transcriptase polymerase chain reaction (qRT-PCR)[13] are the main methods used to detect fusion genes in clinical laboratories. Clinical FISH kits for BCR/ABL^{P210} detection are already available.[14] Based on the precise spatial location, it can distinguish large fragments of chromosomal aberrations rather than specific BCR/ABL^{p210} isoforms. Given the high sensitivity of qRT-PCR, it is applied to quantitatively detect the BCR/ABL^{p210} fusion transcript expression level. However, it cannot distinguish the isoforms of the fusion gene either. Some methods have been established for the simultaneous quantitative detection and isoform analysis of BCR/ABL^{p210} fusion genes. Christopoulos's group reported a dry chemical method based on gold nanoparticles. This method detected cDNA products and required an additional RT-PCR process.[3] cDNA sequencing provided more direct evidence for the identification of e13a2 and e14a2 isoforms. However, it also required the RT-PCR process.[15−17] Our group previously reported an RNA fusion-triggered rolling loop amplification reaction to discern the BCR/ABL^{p210} fusion gene isoforms.[17] This process was carried out in two tubes and also required the participation of enzymes. Therefore, it is necessary to establish a more effective

Received: April 6, 2021
Accepted: July 19, 2021
Published: July 29, 2021

and simple method to identify the fusion gene isoforms in one-pot.

Recently, DNA-templated silver nanoclusters (DNA−AgNCs) have been widely used in biological analysis and imaging as excellent fluorescent nanomaterials due to their good flexibility, stability, and perfect biocompatibility.[18] Altering the DNA template sequence and structure can modulate its emission wavelength spanning from the cyan region (450−492 nm) to the near-infrared region (>700 nm).[19] Especially, an interesting phenomenon was found by Yeh et al. that the fluorescence of AgNCs can be greatly activated when they are placed in proximity to the guanine (G)-rich enhancer sequence, and a binary probe named nanocluster beacon (NCB) was constructed to detect an influenza target.[20] This light-up phenomenon has been successfully applied to detect tumor-specific miRNA,[21] viral DNA,[22] enzymes,[23] and tumor-specific antigens.[24] Moreover, a thymine (T)-rich sequence also has the ability to enhance the fluorescence of AgNCs.[20] These facts provide the possibility to realize multiple detection in the same system by lighting up appropriate DNA−AgNCs. For example, Qu's group reported for the first time a strategy based on multi-color DNA−AgNCs that were lighted up by G-rich and T-rich enhancer sequences for simultaneous fingerprint imaging.[25] However, compared with a G-rich enhancer, the fluorescence enhancement of this DNA−AgNCs template (CCCTTAATCCCC) lit up by T-rich enhancer sequences is not satisfactory due to the high background signal resulting in a low signal-to-background ratio (S/B ratio).[20,25]

Therefore, in this work, we first explored an ideal DNA−AgNCs template sequence with a better S/B ratio after it was lit up by a T-rich enhancer and established a new strategy to detect fusion gene isoforms, e14a2 and e13a2, in one-pot by forming a three-way junction (3-WJ) structure. We found that the dark DNA−AgNCs (CCTCCTTCCTCC) can be enhanced by both T-rich and G-rich sequences with a good enhancement effect. Then, we took advantage of this AgNCs as a signal reporter molecule and designed two bifunctional tuning probes which contain the enhancer sequences (G-rich or T-rich) and the recognition sequence of the corresponding isoforms. In the presence of the corresponding target, the signal reporter of AgNCs will be pulled closer to the corresponding enhancer sequence, generating the characteristic wavelength fluorescence. Thus, the corresponding isoforms can be identified by distinguishing two non-overlapping fluorescence peaks. In general, our strategy provides a simple and enzyme-free method for the simultaneous detection of the fusion gene isoforms, e14a2 and e13a2, in one step, which is of great potential value in clinical applications for CML diagnosis and treatment.

2. MATERIALS AND METHODS

2.1. Reagents and Materials. HPLC-purified DNA oligonucleotides (Table S1), diethylpyrocarbonate (DEPC), and dimethyl sulfoxide (DMSO) were obtained from Sangon Biotechnology Co., Ltd. (Shanghai, China). Silver nitrate ($AgNO_3$) and sodium borohydride ($NaBH_4$) were obtained from Sigma-Aldrich Co., Ltd. (St. Louis, USA). Ultrapure water (Millipore, resistivity, over 18.2 MΩ) was used in all the experiments. Tubes and tips were all RNase-free. All other reagents in the experiment were of analytical grade.

2.2. Apparatus. A Cary Eclipse fluorescence spectrophotometer (Agilent Technologies, USA) was used in the experiment to measure the fluorescence intensity. A Talos F200X transmission electron microscopy (TEM) instrument (Thermo Fisher Scientific, USA) was used to characterize the size of DNA−AgNCs. Polyacrylamide gel electrophoresis was performed on a Bio-Rad electrophoresis analyzer (Bio-Rad, USA) and imaged on a Bio-Rad ChemDoc XRS (Bio-Rad, USA). A UV-2550 spectrophotometer (Shimadzu, Japan) was used in the experiment to measure UV−vis absorption spectra. A NanoDrop spectrophotometer (Thermo Fisher Scientific Inc. Waltham Mass, USA) was used to measure the concentration of extracted total RNA.

2.3. Synthesis of DNA−AgNCs. The DNA template sequences AgNCs−ABL, AgNCs-1, and AgNCs-2 were used to synthesize DNA−AgNCs according to the previous report with some changes.[26] 20 μL of the DNA template sequence (20 μM), 12 μL of $AgNO_3$ (300 μM), and 156 μL of 2 × PBS (PH 7.0) were mixed together. Then, the mixture of DNA and $AgNO_3$ was vortexed for 30 s and then centrifuged at 10 000 rpm for 30 s. Next, the mixture was incubated at 4 °C for at least 15 h to stabilize the AgNCs on the DNA strand. 12 μL of $NaBH_4$ (300 μM) was added to the incubated Ag−DNA mixture. Finally, the mixture was incubated at 25 °C in a metal bath for 5 h and stored at 4 °C for future use. The molar reaction ratio in this experiment was DNA/$AgNO_3$/$NaBH_4$ = 1:9:9 (final concentrations were 2, 18, and 18 μM, respectively).

2.4. Sample Preparation. Chronic myelogenous leukemia cell lines K562 and KCL22, obtained from the First Affiliated Hospital of Chongqing Medical University, were cultured in RPMI 1640 medium in a humidified incubator (5% CO_2 filled) at 37 °C supplemented with 10% fetal bovine serum, 1% streptomycin, and 1% penicillin. The cells were gathered into a centrifuge tube and centrifuged at 700 rpm for 3 min, the supernatant was discarded, an appropriate volume of PBS was added, and repeatedly washed three times. Peripheral blood samples were collected from 16 healthy volunteers with informed consent. The First Affiliated Hospital of Chongqing Medical University approved the collection and use of samples. The red blood cells in peripheral blood were lysed with the Hayem cell lysis solution. The leukemic cells and normal white blood cells (WBCs) were resuspended with normal saline to count the number of cells. K562 cells and KCL22 cells were mixed with WBCs at different ratios. The bone marrow blood of 13 BCR/ABL^{P210} positive patients and 6 non-leukemic patients were obtained with informed consent. Ethics approval was obtained for this research from the Medical Ethics Committee of the First Affiliated Hospital of Chongqing Medical University (NSFC81873972). Hayem's solution with 0.14 M ammonium chloride and 0.02 M Tris was used to obtain isolated mononuclear cells. Then, the total RNA was extracted with the TRIzol reagent.

2.5. Hybridization of DNA−AgNCs and Enhancer Sequences. Different control groups (the final concentrations of all probes were 1 μM) were prepared. After vigorously shaking for 1 min, the samples were incubated at 37 °C for 40 min. The absorption spectrum of each group was recorded in the range from 800 to 350 nm to find absorption peaks for the dark state and the bright state of DNA−AgNCs. Then, the absorption peaks were used as the excitation wavelength to determine their emission peaks.

The light-up effect was estimated using the S/B ratio, the calculation method was that the fluorescence intensity of the bright state formed after hybridization with the enhancer sequence was defined as the signal and the fluorescence intensity of the dark state of the silver cluster itself was defined as the background signal. The S/B ratio is the ratio of the signal to the background signal.

2.6. Simultaneous One-Step Detection. For mimic DNA or cell extracts: 50 μL of prepared AgNCs−ABL (600 nM), 5 μL of e13a2-T12 (6 μM), 5 μL of e14a2-G4 (6 μM), 5 μL of different concentrations of e13a2 and e14a2 (or the corresponding RNA extracts), and 2 × PBS (PH 7.0) were mixed together in a total volume of 100 μL. The sample was incubated in the metal bath at 37 °C for 40 min. Then, the emission fluorescence signals were measured in the wavelength range from 460 to 800 nm with 450 nm excitation wavelength for e13a2 and from 605 to 750 nm with 595 nm excitation wavelength for e14a2 at room temperature under optimal experimental conditions. The voltage was 700 V.

For bone marrow blood samples: 50 μL of prepared AgNCs−ABL (600 nM), 5 μL of e13a2-T12 (6 μM), 5 μL of e14a2-G4 (6 μM), 30

https://doi.org/10.1021/acssensors.1c00695
ACS Sens. 2021, 6, 2928−2937

Scheme 1. (A) Formation Mechanism of e13a2 and e14a2 Isoforms of the BCR/ABL^{P210} Fusion Gene; (B) Schematic Diagram of the Simultaneous Detection of e13a2 and e14a2 Isoforms of BCR/ABL^{P210} Fusion Genes

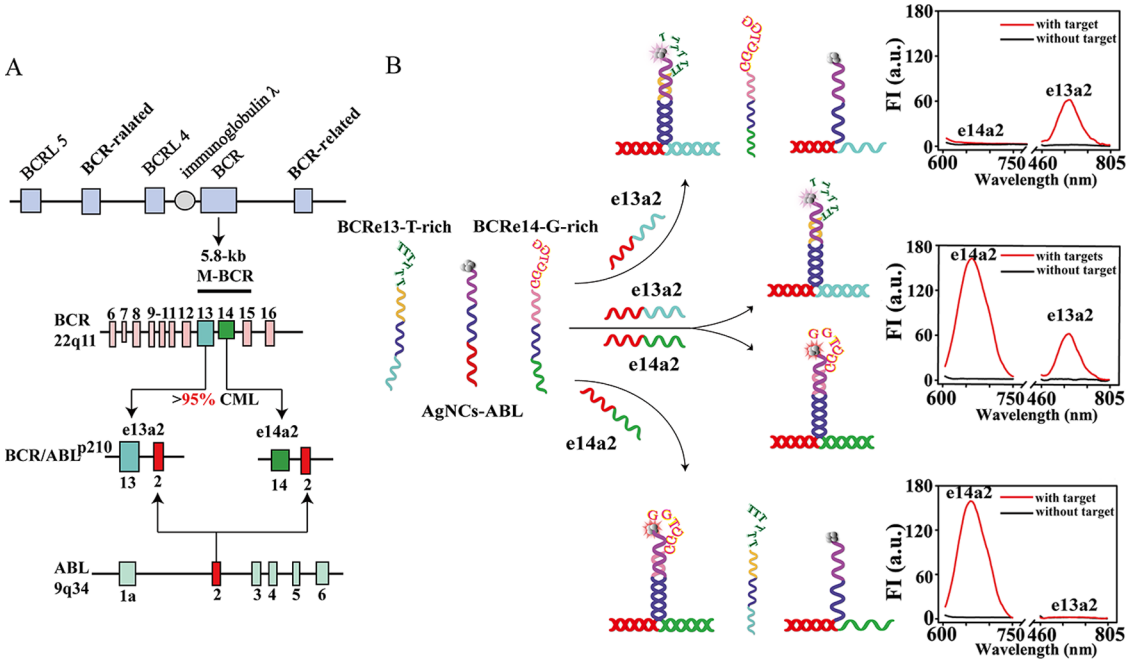

μL of RNA extracts (40 ng/μL), and 2 × PBS (PH 7.0) were mixed together in a total volume of 100 μL. The sample was incubated in the metal bath at 37 °C for 40 min. Then, the emission fluorescence signals were measured in the wavelength range from 460 to 800 nm with 450 nm excitation wavelength for e13a2 and from 605 to 750 nm with 595 nm excitation wavelength for e14a2 at room temperature under optimal experimental conditions. The voltage was 800 V.

2.7. Native Polyacrylamide Gel Electrophoresis. To verify the feasibility of our strategy, the products and the oligonucleotides of the strategy were analyzed by 12% native polyacrylamide gel electrophoresis (PAGE) in 1 × TBE buffer (90 mM Tris−HCl, 90 mM boric acid, and 2 mM EDTA; pH, 7.9) at 110 V for 30 min and then the photo of the gel was taken by a Bio-Rad ChemDoc XRS.

3. RESULTS AND DISCUSSION

3.1. Principle of the Strategy. In this work, a fast and simple strategy based on NCB was proposed to identify both e13a2 and e14a2 simultaneously in one-pot. The fusion mechanism is presented in Scheme 1A, exon 2 of the ABL gene at chromosome 9 fused with exon 13 or exon 14 of the BCR gene at chromosome 21 to form e13a2 and e14a2 isoforms, respectively. Different breakpoints lead to the formation of different subtypes, which is also the key point of identification. Only when the recognition site and the fusion site matched perfectly, specificity of our strategy can be guaranteed. Information about the BCR/ABL^{P210} fusion genes is given in the Supporting Information. As shown in Scheme 1B, the efficient 3-WJ structure was used to detect the fusion gene, which was expected to be assembled by the AgNC signal reporter, target, and tuning sequence. To be specific, the AgNC signal reporter contains a 5 nt "stem" structure, which can bring the turning probe proximal to AgNCs, and is flanked by the 20 nt ABL gene recognition domain and the 12 nt DNA−AgNCs templating domain (named AgNCs−ABL probe). Two kinds of tuning sequences, one composed of the 20 nt BCRe13 recognition domain and the 12 nt T-rich enhancement domain (named BCRe13-T-rich probe) and the other composed of the 20 nt BCRe14 recognition domain and the 18 nt G-rich enhancement domain (named BCRe14-G-rich probe). They also share 5 nt "stem" structures with its neighbor AgNCs−ABL. When the corresponding isoforms exists, the AgNCs−ABL probe and the corresponding BCRe13-T-rich or BCRe14-G-rich probe will be close to each other, which then hybridize with the fusion gene to form a stable 3-WJ structure. Therefore, AgNCs will light up and produce fluorescence with different wavelengths after being enhanced by G-rich or T-rich sequences, which represent the corresponding isoforms.

3.2. Exploration of the DNA−AgNCs Template. In this strategy, the DNA−AgNCs template was expected to emit different wavelengths of fluorescence after being illuminated by G-rich or T-rich enhancer sequences to distinguish the two BCR/ABL^{P210} fusion gene isoforms. According to a previous report, the DNA−AgNCs template sequence CCCTTAATCCCC (AgNCs-1) can be enhanced by the G-rich and T-rich enhancer sequences simultaneously.[20] However, the effect of this template enhanced by the T-rich enhancer sequence was not satisfactory, which cannot meet the requirement of detection sensitivity. Therefore, it is necessary to choose an ideal DNA−AgNCs template sequence which can be greatly enhanced by both G-rich and T-rich sequences to distinguish BCR/ABL^{P210} fusion genes simultaneously. In the experiment, we found that the DNA−AgNCs template CCTCCTTCCTCC (AgNCs-2) can be enhanced by the T-rich sequence with a good S/B ratio and a low background signal. At the same time, it also shows a good enhancement effect by the G-rich sequence.[27] More importantly, these DNA−AgNCs can release different wavelengths of fluorescence without overlapping each other after being enhanced by G-rich and T-rich sequences.

We first studied UV absorption spectra of this specific AgNCs-2 before and after being in proximity to G-rich and T-rich enhancer sequences. As shown in Figure 1A, AgNCs-2 (curve a) showed an absorption peak at around 420 nm, which was the result of the surface plasmon resonance peak for the

https://doi.org/10.1021/acssensors.1c00695
ACS Sens. 2021, 6, 2928−2937

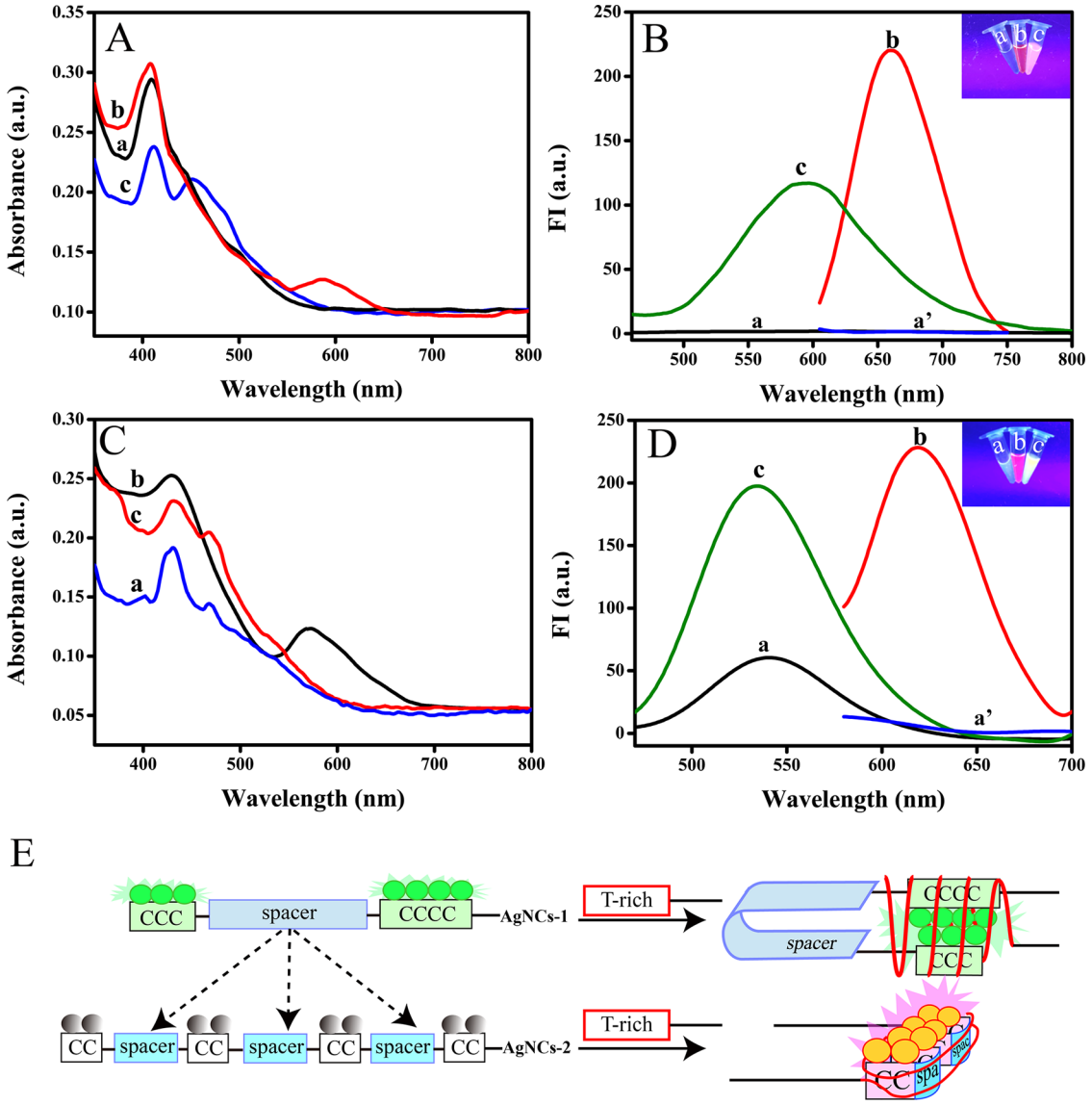

Figure 1. (A) Absorption spectra of AgNCs-2 (a), AgNCs-2 + G-rich-enhancer (b), and AgNCs-2 + T-rich-enhancer (c). (B) Fluorescence spectra of AgNCs-2 (a, λ_{ex} = 450 nm; a', λ_{ex} = 595 nm), AgNCs-2 + G-rich-enhancer (b, λ_{ex} = 595 nm), and AgNCs-2 + T-rich-enhancer (c, λ_{ex} = 450 nm), inset: the color of the samples under a UV lamp. (C) Absorption spectra of AgNCs-1 (a), AgNCs-1 + G-rich-enhancer (b), and AgNCs-1 + T-rich-enhancer (c). (D) Fluorescence spectra of AgNCs-1 (a, λ_{ex} = 460 nm; a', λ_{ex} = 570 nm), AgNCs-1 + G-rich-enhancer (b, λ_{ex} = 570 nm), and AgNCs-1 + T-rich-enhancer (c, λ_{ex} = 460 nm). Inset: the color of the samples under a UV lamp. (E) Potential mechanism of T-rich enhancement.

Ag nanoparticles (AgNPs).[21] Besides this peak, AgNCs-2 hybridized with the G-rich-enhancer (AgNCs-2/G-rich-enhancer) showed a new broad absorption peak at 595 nm (curve b), while AgNCs-2 hybridized with a T-rich-enhancer (AgNCs-2/T-rich-enhancer) showed a distinct wide absorption peak at 450 nm (curve c). This apparently confirmed that AgNCs-2 had distinct enhancement effects when placed with different enhancer sequences. As shown in Figure 1B, when excited at 450 nm, the fluorescence intensity of the AgNCs-2/T-rich-enhancer showed a maximum emission at 600 nm (curve c), which was greatly increased than that of only AgNCs-2 (curve a). When excited at 595 nm, the emission maxima of AgNCs-2/G-rich enhancer was at 663 nm (curve b), while no fluorescence emission occurred for AgNCs-2 (curve a'). This phenomenon was also demonstrated under a UV lamp (inset of Figure 1B). AgNCs-2/G-rich enhancer generated a deep red fluorescence, while the AgNCs-2/T-rich enhancer generated a strong pink fluorescence. The above results indicated that AgNCs-2 had an excellent signal amplification efficiency after being enhanced by G-rich or T-rich sequences. Furthermore, we also compared the enhancement effect of AgNCs-2 and AgNCs-1, which has been reported to be enhanced by both G-rich and T-rich sequences at the same time. As shown in Figure 1C,D, we found that AgNCs-1 itself had a high background signal before being enhanced by the T-rich sequence, which leads to a relatively low S/B ratio. In contrast, the AgNCs-2 has a better effect after being enhanced by a T-rich sequence, in which the S/B ratio is 17.2 times more than that of AgNC-1. According to the reference, the detailed mechanism of the light-up phenomenon manifested a spacer sequence (A or T in C-rich domain) spatially separating the AgNCs into small parts to stay in the dark state (low fluorescence intensity) and a G-rich enhancer sequence folding them together in the bright state (high fluorescence intensity).[26] Thus, we speculate that this sequence can be enhanced by a T-rich sequence in which

https://doi.org/10.1021/acssensors.1c00695
ACS Sens. 2021, 6, 2928−2937

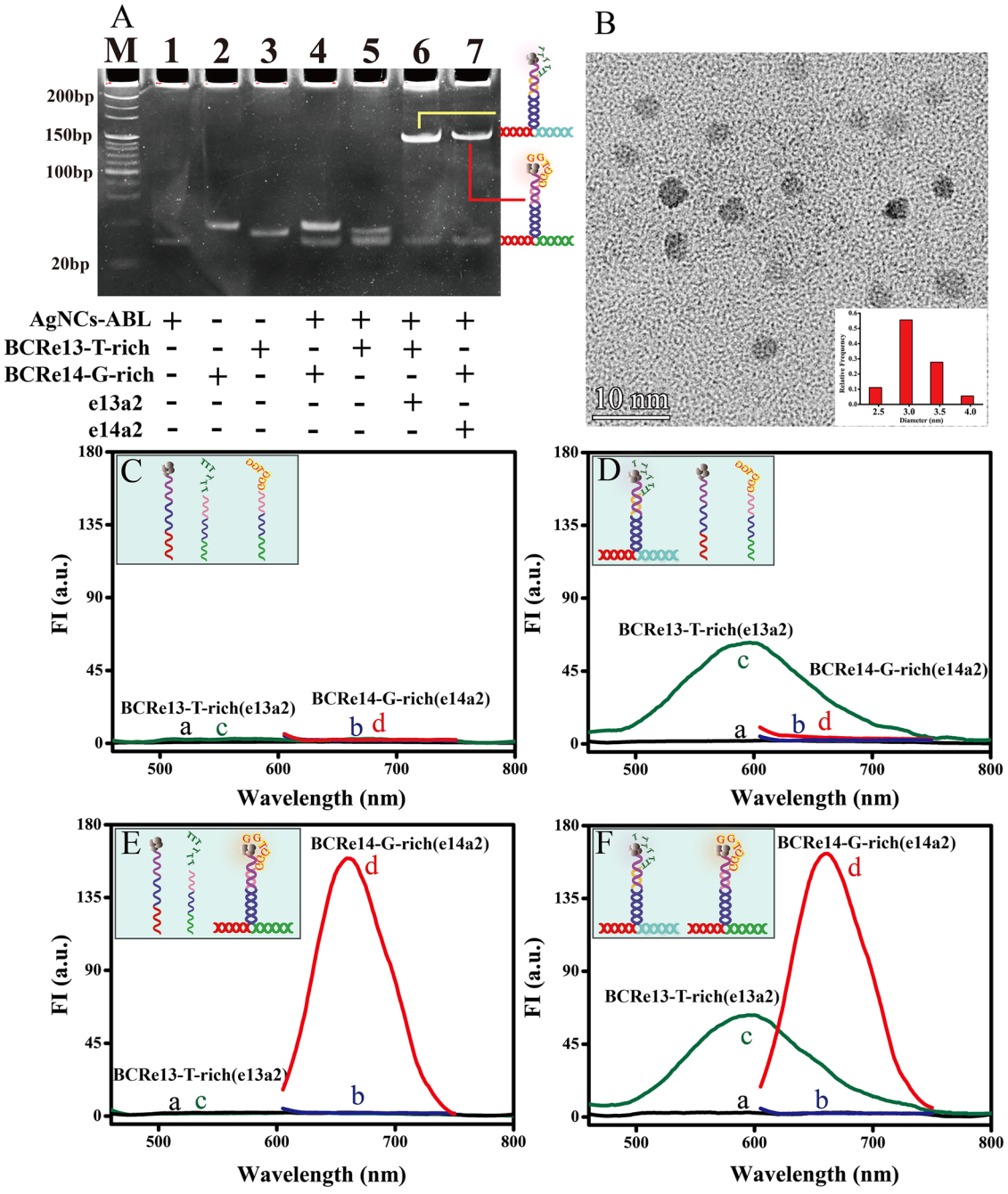

Figure 2. (A) Results of 12% PAGE. (1) AgNCs−ABL, (2) BCRe14-G-rich, (3) BCRe13-T-rich, (4) AgNCs−ABL + BCRe14-G-rich, (5) AgNCs−ABL + BCRe13-T-rich, (6) AgNCs−ABL + BCRe13-T-rich + e13a2, and (7) AgNCs−ABL + BCRe14-G-rich + e14a2. The concentrations of oligonucleotides were all 2 μM. (B) TEM result of AgNCs−ABL. The fluorescence spectra of the detection system without (a,b) and with (c,d): (C) blank, (D) e13a2, (E) e14a2, and (F) e13a2 and e14a2, respectively (a,c, λ_{ex} = 450 nm; b, d, λ_{ex} = 595 nm). The concentrations of e13a2 and e14a2 were 80 nM.

multiple spacers in this DNA−AgNCs template sequence can divide AgNCs into smaller parts, and a T-rich enhancer sequence would have a similar effect in bridging the small AgNCs together (Figure 1E). Considering the balance of the enhancement effect of AgNCs by a T-rich sequence or G-rich sequence, we believe that AgNCs-2 was a superior choice with a stronger enhancement effect both for G-rich and T-rich sequences, which is beneficial to the detection of BCR/ABL^{p210} fusion gene simultaneously in one-pot.

3.3. Feasibility of the Strategy for Multiplex Detection. On the basis of the above turn-on effect observations, we combined the AgNCs-2 template sequence with the ABL gene recognition sequence to form bifunctional AgNCs−ABL probes to identify the BCR/ABL^{p210} fusion gene. First, the PAGE experiment was used to demonstrate the construction of 3-WJ structures. As shown in Figure 2A, no new bands appeared when AgNCs−ABL was incubated with BCRe14-G-rich (lane 4) or BCRe13-T-rich (lane 5), indicating the "stem" structure used to bring an enhancer sequence and AgNCs−ABL together did not work when there was no target. When e13a2 was incubated with AgNCs−ABL and BCRe13-T-rich (lane 6), a brighter band with a larger molecular weight

https://doi.org/10.1021/acssensors.1c00695
ACS Sens. 2021, 6, 2928−2937

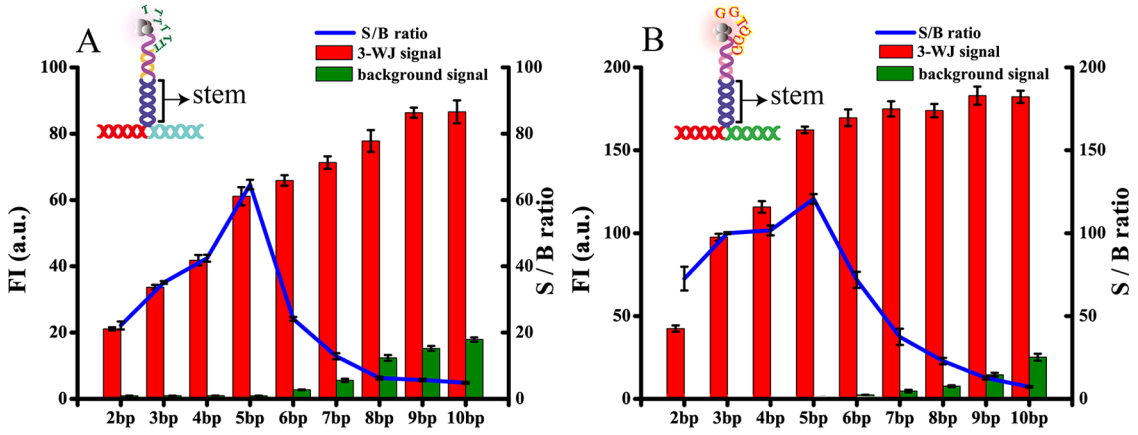

Figure 3. Optimization of base pair numbers of stem. (A) Fluorescence intensity (left axis) with e13a2, without e13a2, and S/B ratio (right axis) of different stem lengths based on T-rich enhancement (λ_{ex} = 450 nm). (B) Fluorescence intensity (left axis) with e14a2, without e14a2, and S/B ratio (right axis) of different stem lengths based on G-rich enhancement (λ_{ex} = 595 nm). The concentrations of e13a2 and e14a2 were 80 nM.

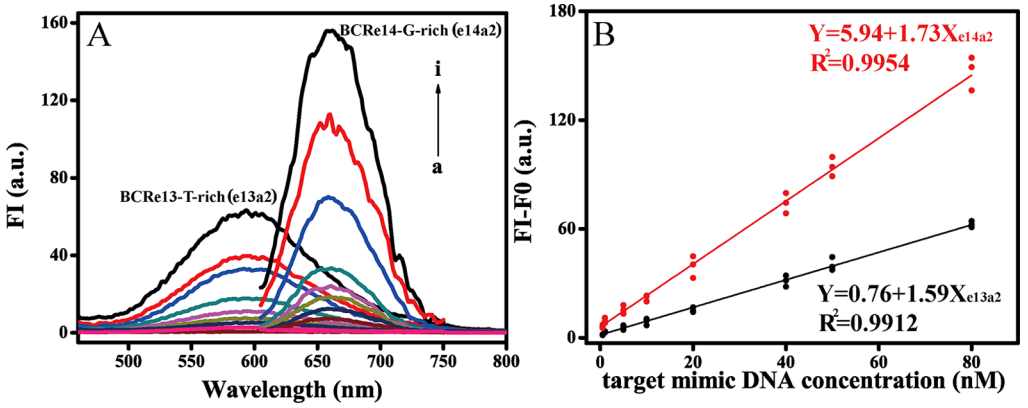

Figure 4. (A) Fluorescence spectra responding to a−i (0, 0.5, 1, 5, 10, 20, 40, 50, and 80 nM respectively) of e13a2 (left, λ_{ex} = 450 nm) and e14a2 (right, λ_{ex} = 595 nm). (B) Calibration curves of the FI−F0 *vs* concentration of target mimic DNA, where FI and F0 represent the fluorescence intensity with and without the target.

emerged, while e14a2 incubated with AgNCs−ABL and BCRe14-G-rich (lane 7) showed a similar clear band. These bands stained with dye gave straightforward evidence of the assembly of a stable 3-WJ structure. Different from silver chloride nanoparticles,[28] the size and the shape of DNA−AgNC particles are restricted by the DNA template.[29] As shown in Figure 2B, the uniform particles of AgNCs−ABL were around 3 nm, which was consistent with a previous report.[30] Meanwhile, the prepared AgNCs−ABL was regularly spherical and well dispersed with a narrow size distribution, which were perfectly adequate for biosensing applications.

To verify the feasibility when AgNCs−ABL, BCRe13-T-rich, and BCRe14-G-rich existed in a tube, their fluorescence responses with or without targets were recorded by exciting each group at 450 and 595 nm, respectively. As shown in Figure 2C, when in the absence of targets e13a2 and e14a2, almost no fluorescence enhancement was found neither at 600 nor at 663 nm (curve c and curve d), respectively. This indicated that when in the absence of the targets e13a2 and e14a2, the background signal of AgNCs−ABL was extremely low and had a negligible effect on the analytical performance. However, when one kind of fusion gene was presented, as shown in Figure 2D , the presence of e13a2 caused the largely increased fluorescence emission at 600 nm (curve c) and an almost constant fluorescence at 663 nm (curve d). When only e14a2 existed (Figure 2E), low emission at 600 nm (curve c) and strong enhancement at 663 nm occurred (curve d). As shown in Figure 2F, the spectra were measured when e13a2 and e14a2 were added simultaneously. The fluorescence amplified significantly at 600 nm (curve c) and 663 nm (curve d), respectively. The above results manifested that the increase of fluorescence at different emission wavelengths accurately corresponded with BCR/ABL^{p210} isoforms.

The excitation spectra were completely non-overlapping at 450 and 595 nm, which corresponded to the simultaneous addition of e13a2 and e14a2, respectively (Figure S1). This result further proved the feasibility of simultaneous detection in one-pot. Furthermore, at the e13a2 detection channel (λ_{ex} = 450 nm), the fluorescence of e13a2 was not affected by the addition of various concentrations of e14a2 (Figure S2). In addition, a similar trend was found for the e14a2 channel (λ_{ex} = 595 nm) (Figure S3). Thus, even though the concentrations of interference targets were significantly greater, the response signal of targets was still impervious to it. The above experimental results verified that we successfully applied the AgNC-2 sequence to leukemia fusion gene detection with its strong dual enhancer sequence turning effect, and the proposed 3-WJ structure-based strategy was feasible and reliable for the simultaneous detection of BCR/ABL^{p210} fusion genes.

https://doi.org/10.1021/acssensors.1c00695
ACS Sens. 2021, 6, 2928−2937

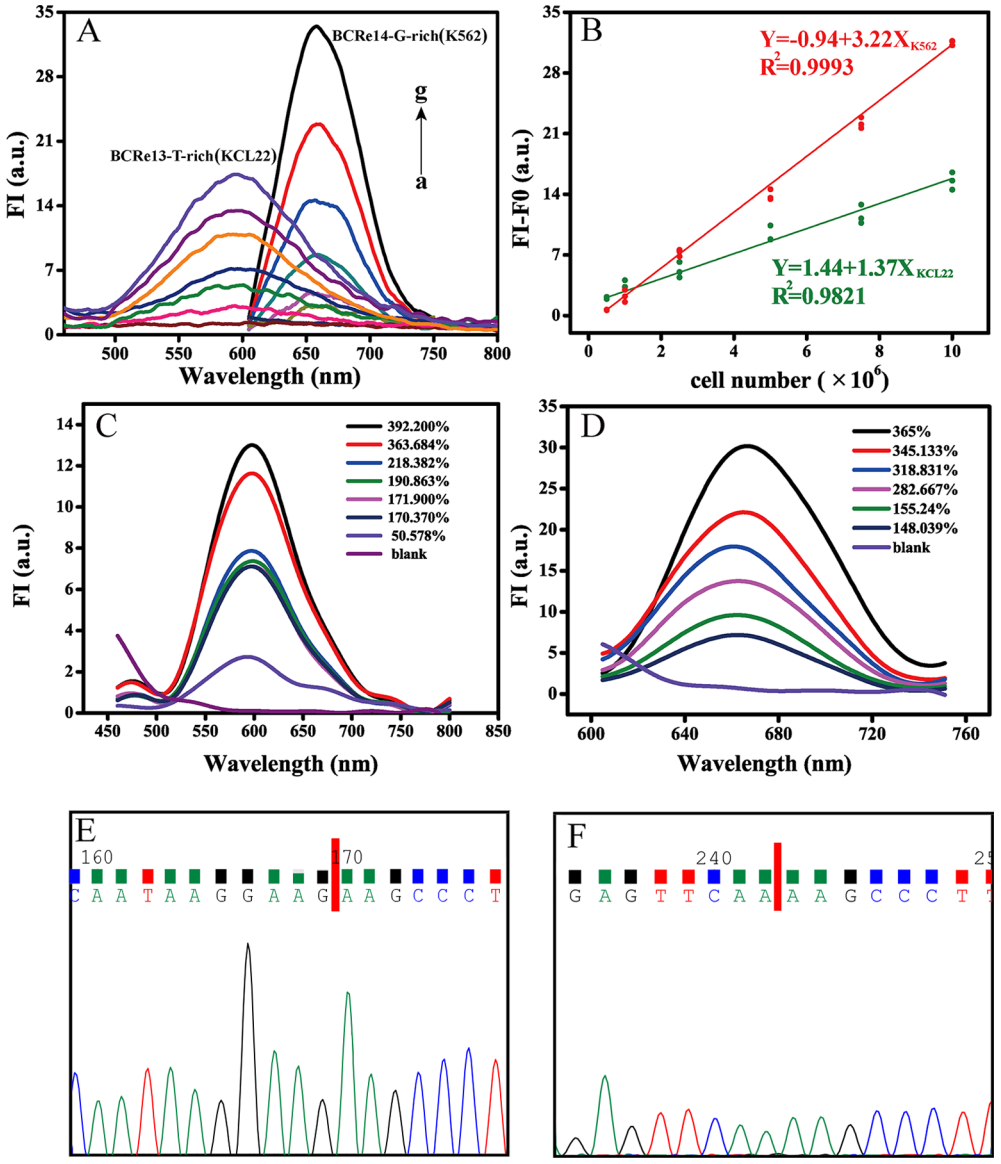

Figure 5. (A) Fluorescence spectra of the detection system responding to 0, 5, 10, 25, 50, 75, and 100% KCL22 (left, λ_{ex} = 450 nm) and K562 cells (right, λ_{ex} = 595 nm) mixed with WBCs in 10^7 total cells. (B) Calibration curves of FI−F0 *vs* cell number, where FI and F0 represent the fluorescence intensity with and without RNA extracts, respectively. Fluorescence curves of newly diagnosed CML patients of e13a2 (C) and e14a2 (D) isoforms. The representative cDNA sequencing graph of newly diagnosed CML patients for e13a2 (E) and e14a2 (F) isoforms. The fusion location is marked with red lines.

3.4. Optimization of the Strategy. Before further application on RNA transcripts, mimic DNA targets were first used to optimize the NCB probe.[31,32] As shown in Figure 3A, the obtained S/B ratio increased when the base number of "stem" increased, and it reached the maximum value at 5 bp. Then, the S/B ratio decreased rapidly due to the increased background signal. As shown in Figure 3B, a similar trend is found for "stem" number optimization of the G-rich enhancement in which 5 bp gave rise to the highest S/B ratio. Therefore, 5 bp was considered as the best length of "stem" both for G-rich and T-rich enhancements. We also investigated other reaction conditions which had an influence on the turn-on performance of DNA−AgNCs. The best values are listed below: the pH of the hybridization solution was 7.0 (Figure S4A); the reaction ratio for DNA−AgNCs synthesis was DNA/$AgNO_3$/$NaBH_4$ 1:9:9 (Figure S4B); the hybridization time was 40 min (Figure S4C); and the hybridization temperature was 37 °C (Figure S4D). As shown in Figure S4E,F, the DNA−AgNCs synthesized in PBS and ultrapure water had similar turn-on fluorescence, and PBS achieved a higher S/B ratio compared with DNA−AgNCs synthesized in ultrapure water.

3.5. Sensitivity of the Strategy. In order to investigate the sensitivity of the strategy, two targets with different concentrations, ranging from 0 to 80 nM were added separately under optimized conditions. As shown in Figure 4A , a significant increase in F−F0 was observed when higher concentrations of the corresponding mimic DNA targets were added. As shown in Figure 4B, the fluorescence of both e13a2 and e14a2 revealed a perfect linear range from 500 pM to 80 nM with a correlation coefficient of 0.9912 and 0.9954, respectively. The detection limits of e13a2 and e14a2 were 16 and 9 pM, respectively. (Estimated using the $3\sigma/S$ formula, where σ means the standard deviation of the blank control, n =

https://doi.org/10.1021/acssensors.1c00695
ACS Sens. 2021, 6, 2928−2937

10, and S represents the slope of the equation of linear regression). Moreover, we compared the NCB strategy with binary probes listed in Table S2. They shared a similar detection mode to obtain a response signal by pulling two probes close together induced by the target.[33] All these methods required the help of a catalyst or expensive labeling process, while NCB was a label-free[34] strategy. Compared with the NCB probe, the probes based on the fluorescence resonance energy transfer or catalyst have difficulty in achieving simultaneous detection. In addition, the NCB strategy showed a lower detection limit than these binary probes.

3.6. Strategy in Complex Matrices. According to a previous report, KCL22 cells expressed e13a2[35] and K562 cells expressed e14a2.[36] To investigate the sensitivity of the strategy in complex matrices, a series of ratio percentages of K562 or KCL22 cells were added to WBCs with a total number of 10^7 cells, respectively. As shown in Figure 5A, the fluorescence signal enhanced gradually with the addition of RNA extractions from higher cell numbers. As shown in Figure 5B , the linear calibration curves presented by the corresponding F−F0 *versus* the number of leukemic cells were displayed with a good correlation. Moreover, besides RNA extraction from leukemia cells, the synthesized mimic DNA e13a2, e14a2, normal ABL, normal BCRe13, and non-complementary sequence (NC) were tested, respectively, to evaluate specificity. As shown in Figure S5A, only the addition of e13a2 mimic sequence and RNA extraction from KCL22 cells significantly enhanced the fluorescence signal at the e13a2 channel. In addition, the e14a2 channel gave rise to similar results that the fluorescence signal increased only for the e14a2 mimic sequence and RNA extraction from K562 cells (Figure S5B).

To further evaluate clinical applications, we gathered RNA extracts of bone marrow blood samples from 13 newly diagnosed CML patients and 6 non-leukemic patients. All CML patients were proved to be BCR/ABL^{P210} positive by a commercialized RT-PCR kit. All BCR/ABL^{P210} positive patients can be successfully classified into e13a2 or e14a2 isoforms with the proposed method, while BCR/ABL^{P210} negative samples from non-leukemic patients were negative in e13a2/e14a2 isoforms (Figure 5C,D). All these results were confirmed with cDNA-sequencing (Figure 5E,F and Table S3). Furthermore, as shown in Figure 5C,D, fluorescence intensities of NCB increased with the increased ratio of BCR/ABL^{P210}/ABL copies obtained with RT-PCR,[37] demonstrating good coincidence of the two methods. Obviously, our strategy directly distinguished isoforms from newly diagnosed CML patients without a reverse transcription process, suggesting the promising potential for further clinical applications.

4. CONCLUSIONS

In summary, we found a DNA−AgNCs template CCTCCTTCCTCC which had strong emission signals modulated by enhancer sequences T-rich and G-rich without overlapping. Then, this DNA−AgNCs template was applied to develop a cost-effective and time-saving fluorescence strategy for simultaneous identification of leukemia isoforms based on NCB. Unlike the qRT-PCR strategy, it perfectly achieved stable and simultaneous BCR/ABL isoform determination without reverse transcription and procedural cooling processes. The detection limits of e13a2 and e14a2 were down to 16 and 9 pM, respectively, and 5% fusion transcripts were successfully discriminated in complex RNA extractions. e13a2 and e14a2 isoforms from newly diagnosed CML patients were successfully identified by the NCB method. This strategy showed tremendous potential to fabricate a simultaneous assay for early clinical diagnosis, therapy, and prognosis of CML.

■ ASSOCIATED CONTENT

Supporting Information

The Supporting Information is available free of charge at https://pubs.acs.org/doi/10.1021/acssensors.1c00695.

Oligonucleotides sequences used in this work, optimization of reaction conditions, and additional data of detection performance for the NCB probe (PDF).

■ AUTHOR INFORMATION

Corresponding Authors

Yuhong Zhang − *The Center for Clinical Molecular Medical Detection, The First Affiliated Hospital of Chongqing Medical University, Chongqing 400016, China*; Phone: +86-23-89011816; Email: Zhangyh1963@126.com; Fax: +86-23-68811487

Wei Cheng − *The Center for Clinical Molecular Medical Detection, The First Affiliated Hospital of Chongqing Medical University, Chongqing 400016, China*; orcid.org/0000-0002-1921-9761; Email: chengwei@hospital.cqmu.edu.cn

Authors

Xiaolong Gou − *The Center for Clinical Molecular Medical Detection, The First Affiliated Hospital of Chongqing Medical University, Chongqing 400016, China*

Lulu Xu − *The Center for Clinical Molecular Medical Detection, The First Affiliated Hospital of Chongqing Medical University, Chongqing 400016, China; The Department of Clinical Laboratory, Shandong Provincial Hospital Affiliated to Shandong First Medical University, Jinan 250021 Shandong, China*

Suqing Yang − *Chongqing Testing & Lnspection Center for Medical Devices, Chongqing 400016, China*

Xiaoxue Cheng − *The Center for Clinical Molecular Medical Detection, The First Affiliated Hospital of Chongqing Medical University, Chongqing 400016, China*

Haiping Wu − *Key Laboratory of Clinical Laboratory Diagnostics (Ministry of Education), College of Laboratory Medicine, Chongqing Medical University, Chongqing 400016, China*

Decai Zhang − *The Center for Clinical Molecular Medical Detection, The First Affiliated Hospital of Chongqing Medical University, Chongqing 400016, China*

Weicheng Shi − *The Center for Clinical Molecular Medical Detection, The First Affiliated Hospital of Chongqing Medical University, Chongqing 400016, China*

Shijia Ding − *Key Laboratory of Clinical Laboratory Diagnostics (Ministry of Education), College of Laboratory Medicine, Chongqing Medical University, Chongqing 400016, China*; orcid.org/0000-0002-9183-1656

Complete contact information is available at: https://pubs.acs.org/10.1021/acssensors.1c00695

Author Contributions

⊥X.G. and L.X. authors contributed equally to this work.

Notes

The authors declare no competing financial interest.

https://doi.org/10.1021/acssensors.1c00695
ACS Sens. 2021, 6, 2928−2937

■ ACKNOWLEDGMENTS

This work was funded by the National Natural Science Foundation of China (81572080 and 81873972), the Natural Science Foundation Project of Chongqing (cstc2015shmszx120086), the Training Program for Advanced Young Medical Personnel of Chongqing (2017HBRC003), the Chongqing Science Fund for Distinguished Young Scholars (cstc2019jcyjjqX0028), and the Foundation for Innovative Research Groups of Chongqing Higher Education Institutions (CXQT20013).

■ REFERENCES

(1) De Klein, A.; Van Agthoven, T.; Groffen, C.; Heisterkamp, N.; Groffen, J.; Grosveld, G. Molecular Analysis of both Translocation Products of a Philadelphia-Positive CML Patient. *Nucleic Acids Res.* **1986**, *14*, 7071−7082.

(2) Champlin, R.; Golde, D. Chronic Myelogenous Leukemia: Recent Advances. *Blood* **1985**, *65*, 1039−1047.

(3) Kalogianni, D. P.; Bravou, V.; Christopoulos, T. K.; Ioannou, P. C.; Zoumbos, N. C. Dry-Reagent Disposable Dipstick Test for Visual Screening of Seven Leukemia-Related Chromosomal Translocations. *Nucleic Acids Res.* **2007**, *35*, No. e23.

(4) Nashed, A. L.; Rao, K. W.; Gulley, M. L. Clinical Applications of Bcr-Abl Molecular Testing in Acute Leukemia. *J. Mol. Diagn.* **2003**, *5*, 63−72.

(5) Oh, E. H.; Jung, S.; Kim, W. J.; Kim, K. P.; Kim, S. K. Microparticle-Based RT-QPCR for Highly Selective Rare Mutation Detection. *Biosens. Bioelectron.* **2017**, *87*, 229−235.

(6) Marley, S. B.; Gordon, M. Y. Chronic Myeloid Leukaemia: Stem Cell Derived But Progenitor Cell Driven. *Clin. Sci.* **2005**, *109*, 13−25.

(7) Melo, J. The Diversity of Bcr-Abl Fusion Proteins And Their Relationship to Leukemia Phenotype. *Blood* **1996**, *88*, 2375−2384.

(8) Deininger, M. W. N.; Goldman, J. M.; Melo, J. V. The Molecular Biology of Chronic Myeloid Leukemia. *Blood* **2000**, *96*, 3343−3356.

(9) Goh, H.-G.; Hwang, J.-Y.; Kim, S.-H.; Lee, Y.-H.; Kim, Y.-L.; Kim, D.-W. Comprehensive Analysis of BCR-ABL Transcript Types in Korean CML Patients Using a Newly Developed Multiplex RT-PCR. *Transl. Res.* **2006**, *148*, 249−256.

(10) Baccarani, M.; Rosti, G.; Soverini, S. Chronic Myeloid Leukemia: the Concepts of Resistance and Persistence and the Relationship with the BCR-ABL1 Transcript Type. *Leukemia* **2019**, *33*, 2358−2364.

(11) Hanfstein, B.; Lauseker, M.; Hehlmann, R.; Saussele, S.; Erben, P.; Dietz, C.; Fabarius, A.; Proetel, U.; Schnittger, S.; Haferlach, C.; Krause, S. W.; Schubert, J.; Einsele, H.; Hänel, M.; Dengler, J.; Falge, C.; Kanz, L.; Neubauer, A.; Kneba, M.; Stegelmann, F.; Pfreundschuh, M.; Waller, C. F.; Spiekermann, K.; Baerlocher, G. M.; Pfirrmann, M.; Hasford, J.; Hofmann, W.-K.; Hochhaus, A.; Müller, M. C. Distinct Characteristics of e13a2 Versus e14a2 Bcr-Abl1 Driven Chronic Myeloid Leukemia under First-Line Therapy With Imatinib. *Haematologica* **2014**, *99*, 1441−1447.

(12) Qadir, M. A.; Zhan, S. H.; Kwok, B.; Bruestle, J.; Drees, B.; Popescu, O.-E.; Sorensen, P. H. ChildSeq-RNA: A Next-Generation Sequencing-Based Diagnostic Assay to Identify Known Fusion Transcripts in Childhood Sarcomas. *J. Mol. Diagn.* **2014**, *16*, 361−370.

(13) Kim, D. H.; Popradi, G.; Sriharsha, L.; Kamel-Reid, S.; Chang, H.; Messner, H. A.; Lipton, J. H. No Significance of Derivative Chromosome 9 Deletion on the Clearance Kinetics of BCR/ABL Fusion Transcripts, Cytogenetic or Molecular Response, Loss of Response, or Treatment Failure to Imatinib Mesylate Therapy for Chronic Myeloid Leukemia. *Cancer* **2008**, *113*, 772−781.

(14) Xu, N.; Li, Y.-l.; Li, X.; Zhou, X.; Cao, R.; Li, H.; Li, L.; Lu, Z.-y.; Huang, J.-x.; Fan, Z.-p.; Huang, F.; Zhou, H.-s.; Zhang, S.; Liu, Z.; Zhu, H.-q.; Liu, Q.-f.; Liu, X.-l. Correlation between Deletion of the CDKN2 Gene and Tyrosine Kinase Inhibitor Resistance in Adult Philadelphia Chromosome-Positive Acute Lymphoblastic Leukemia. *J. Hematol. Oncol.* **2016**, *9*, 40.

(15) Meissner, R. D. V.; Dias, P. M. B.; Covas, D. T.; Job, F.; Leite, M.; Nardi, N. B. A Polymorphism in Exon b2 of the Major Breakpoint Cluster Region (M-bcr) Identified in Chronic Myeloid Leukaemia Patients. *Br. J. Haematol.* **1998**, *103*, 224−226.

(16) Sharma, A.; Pandey, C. M.; Sumana, G.; Soni, U.; Sapra, S.; Srivastava, A. K.; Chatterjee, T.; Malhotra, B. D. Chitosan Encapsulated Quantum Dots Platform for Leukemia Detection. *Biosens. Bioelectron.* **2012**, *38*, 107−113.

(17) Luo, N.; Xia, Q.; Zhang, L.; Zhang, Y.; Huang, L.; Zhang, Y.; Zhao, J.; Ding, S.; Cheng, W. One-Step Discrimination of BCR/ABL Transcript Isoforms Directly from RNA Extraction with Fusion-Triggered Rolling Circle Amplification. *Anal. Chim. Acta* **2019**, *1067*, 129−136.

(18) Obliosca, J. M.; Babin, M. C.; Liu, C.; Liu, Y.-L.; Chen, Y.-A.; Batson, R. A.; Ganguly, M.; Petty, J. T.; Yeh, H.-C. A Complementary Palette of NanoCluster Beacons. *ACS Nano* **2014**, *8*, 10150−10160.

(19) Richards, C. I.; Choi, S.; Hsiang, J.-C.; Antoku, Y.; Vosch, T.; Bongiorno, A.; Tzeng, Y.-L.; Dickson, R. M. Oligonucleotide-Stabilized Ag Nanocluster Fluorophores. *J. Am. Chem. Soc.* **2008**, *130*, 5038−5039.

(20) Yeh, H.-C.; Sharma, J.; Han, J. J.; Martinez, J. S.; Werner, J. H. A DNA–Silver Nanocluster Probe that Fluoresces upon Hybridization. *Nano Lett.* **2010**, *10*, 3106−3110.

(21) Han, Y.; Zhang, F.; Gong, H.; Cai, C. Multifunctional G-quadruplex-Based Fluorescence Probe Coupled with DNA-Templated AgNCs for Simultaneous Detection of Multiple DNAs and Micro-RNAs. *Anal. Chim. Acta* **2019**, *1053*, 105−113.

(22) Zou, R.; Zhang, F.; Chen, C.; Cai, C. DNA-Programming Multicolor Silver Nanoclusters for Sensitively Simultaneous Detection of Two HIV DNAs. *Sens. Actuators, B* **2019**, *296*, 126608.

(23) Li, J.; Ma, J.; Zhang, Y.; Zhang, Z.; He, G. A Fluorometric Method for Determination of the Activity of T4 Polynucleotide Kinase by Using a DNA-Templated Silver Nanocluster Probe. *Mikrochim. Acta* **2019**, *186*, 48.

(24) Xu, X.; Ji, J.; Chen, P.; Wu, J.; Jin, Y.; Zhang, L.; Du, S. Salt-Induced Gold Nanoparticles Aggregation Lights Up Fluorescence of DNA-Silver Nanoclusters to Monitor Dual Cancer Markers Carcinoembryonic Antigen and Carbohydrate Antigen 125. *Anal. Chim. Acta* **2020**, *1125*, 41−49.

(25) Ran, X.; Wang, Z.; Zhang, Z.; Pu, F.; Ren, J.; Qu, X. Nucleic-Acid-Programmed Ag-Nanoclusters as a Generic Platform for Visualization of Latent Fingerprints and Exogenous Substances. *Chem. Commun.* **2016**, *52*, 557−560.

(26) Ang, Y. S.; Woon, W. W. E.; Yung, L.-Y. L. The Role of Spacer Sequence in Modulating Turn-On Fluorescence of DNA-Templated Silver Nanoclusters. *Nucleic Acids Res.* **2018**, *46*, 6974−6982.

(27) Yeh, H.-C.; Sharma, J.; Han, J.; Martinez, J.; Werner, J. A beacon of light: a new molecular probe for homogeneous detection of nucleic acid targets. *IEEE Nanotechnol. Mag.* **2011**, *5*, 28−33.

(28) Kabir, S. R.; Asaduzzaman, A.; Amin, R.; Haque, A. T.; Ghose, R.; Rahman, M. M.; Islam, J.; Amin, M. B.; Hasan, I.; Debnath, T.; Chun, B.-S.; Zhao, X.; Rahman Khan, M. K.; Alam, M. T. Zizyphus Mauritiana Fruit Extract-Mediated Synthesized Silver/Silver Chloride Nanoparticles Retain Antimicrobial Activity and Induce Apoptosis in MCF-7 Cells through the Fas Pathway. *ACS Omega* **2020**, *5*, 20599−20608.

(29) Xu, S.; Jiang, L.; Wang, J.; Gao, Y.; Luo, X. Ratiometric Multicolor Analysis of Intracellular MicroRNA Using a Chain Hybrid Substitution-Triggered Self-Assembly of Silver Nanocluster-Based Label-Free Sensing Platform. *ACS Appl. Mater. Interfaces* **2020**, *12*, 373−379.

(30) Yuan, Y.; Ma, Y.; Luo, L.; Wang, Q.; Huang, J.; Liu, J.; Yang, X.; Wang, K. Ratiometric Determination of Human Papillomavirus-16 DNA by Using Fluorescent DNA-Templated Silver Nanoclusters and Hairpin-Blocked DNAzyme-Assisted Cascade Amplification. *Mikrochim. Acta* **2019**, *186*, 613.

https://doi.org/10.1021/acssensors.1c00695
ACS Sens. 2021, 6, 2928−2937

(31) Yang, Y.; Huang, J.; Yang, X.; Quan, K.; Wang, H.; Ying, L.; Xie, N.; Ou, M.; Wang, K. FRET Nanoflares for Intracellular mRNA Detection: Avoiding False Positive Signals and Minimizing Effects of System Fluctuations. *J. Am. Chem. Soc.* **2015**, *137*, 8340−8343.
(32) He, L.; Lu, D.-Q.; Liang, H.; Xie, S.; Luo, C.; Hu, M.; Xu, L.; Zhang, X.; Tan, W. Fluorescence Resonance Energy Transfer-Based DNA Tetrahedron Nanotweezer for Highly Reliable Detection of Tumor-Related mRNA in Living Cells. *ACS Nano* **2017**, *11*, 4060−4066.
(33) Kolpashchikov, D. M. Binary Probes for Nucleic Acid Analysis. *Chem. Rev.* **2010**, *110*, 4709−4723.
(34) Zhang, Y.; Mu, F.; Duan, Y.; Li, Q.; Pan, Y.; Du, H.; He, P.; Shen, X.; Luo, Z.; Zhu, C.; Wang, L. Label-Free Analysis of H5N1 Virus Based on Three-Segment Branched DNA-Templated Fluorescent Silver Nanoclusters. *ACS Appl. Mater. Interfaces* **2020**, *12*, 48357−48362.
(35) Rapozzi, V.; Xodo, L. E. Efficient Silencing of Bcr/abl Oncogene by Single- and Double-Stranded siRNAs Targeted Against b2a2 Transcripts. *Biochemistry* **2004**, *43*, 16134−16141.
(36) Mundhada, S.; Luthra, R.; Cano, P. Association of HLA Class I and Class II Genes with Bcr-Abl Transcripts in Leukemia Patients with t(9;22) (q34;q11). *BMC Canc.* **2004**, *4*, 25.
(37) O'Brien, S.; Berman, E.; Borghaei, H.; Deangelo, D. J.; Devetten, M. P.; Devine, S.; Erba, H. P.; Gotlib, J.; Jagasia, M.; Moore, J. O.; Mughal, T.; Pinilla-Ibarz, J.; Radich, J. P.; Shah, N. P.; Shami, P. J.; Smith, B. D.; Snyder, D. S.; Tallman, M. S.; Talpaz, M.; Wetzler, M. NCCN Clinical Practice Guidelines in Oncology: Chronic Myelogenous Leukemia. *J. Natl. Compr. Canc. Netw.* **2009**, *7*, 984−1023.

https://doi.org/10.1021/acssensors.1c00695
ACS Sens. 2021, 6, 2928−2937